在那遙遠的地方

江瑛貴
國立清華大學
物理系/天文所

Outline

1. 物理 (實驗，理論)
2. 天文 (觀測)
3. 天文物理 (觀測, 理論, 電腦模擬, 實驗)
4. 內容簡介，特質
5. 巡天觀測研究室: People, Projects

Galaxy NGC 4639

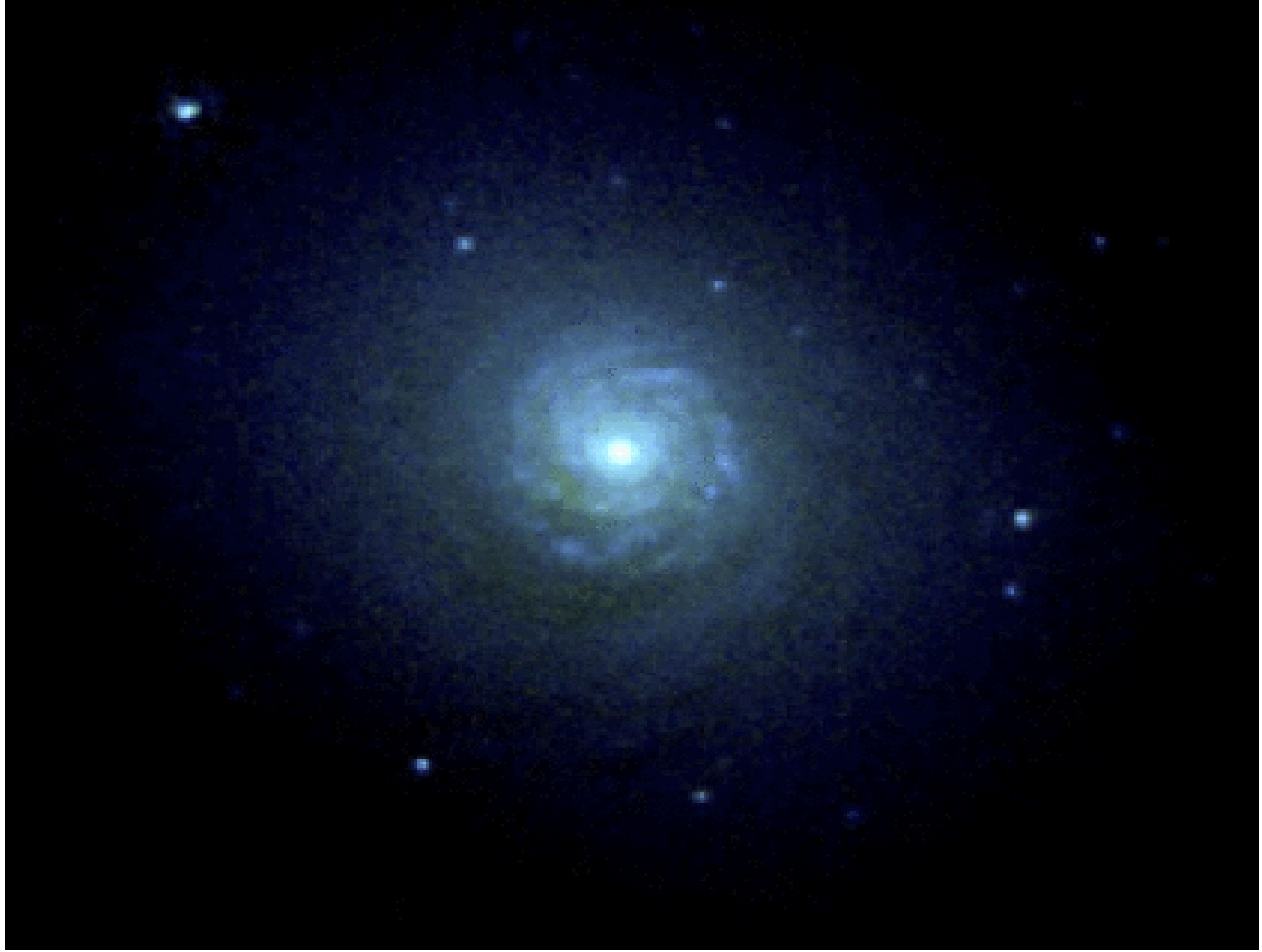

Nucleus of Galaxy NGC 7252

NASA Hubble Space Telescope image of the core of the peculiar galaxy NGC 7252 reveals a striking "mini-spiral" disk of gas and stars, and about 40 exceptionally bright and young globular star clusters. The visible light image was taken with the Wide Field and Planetary

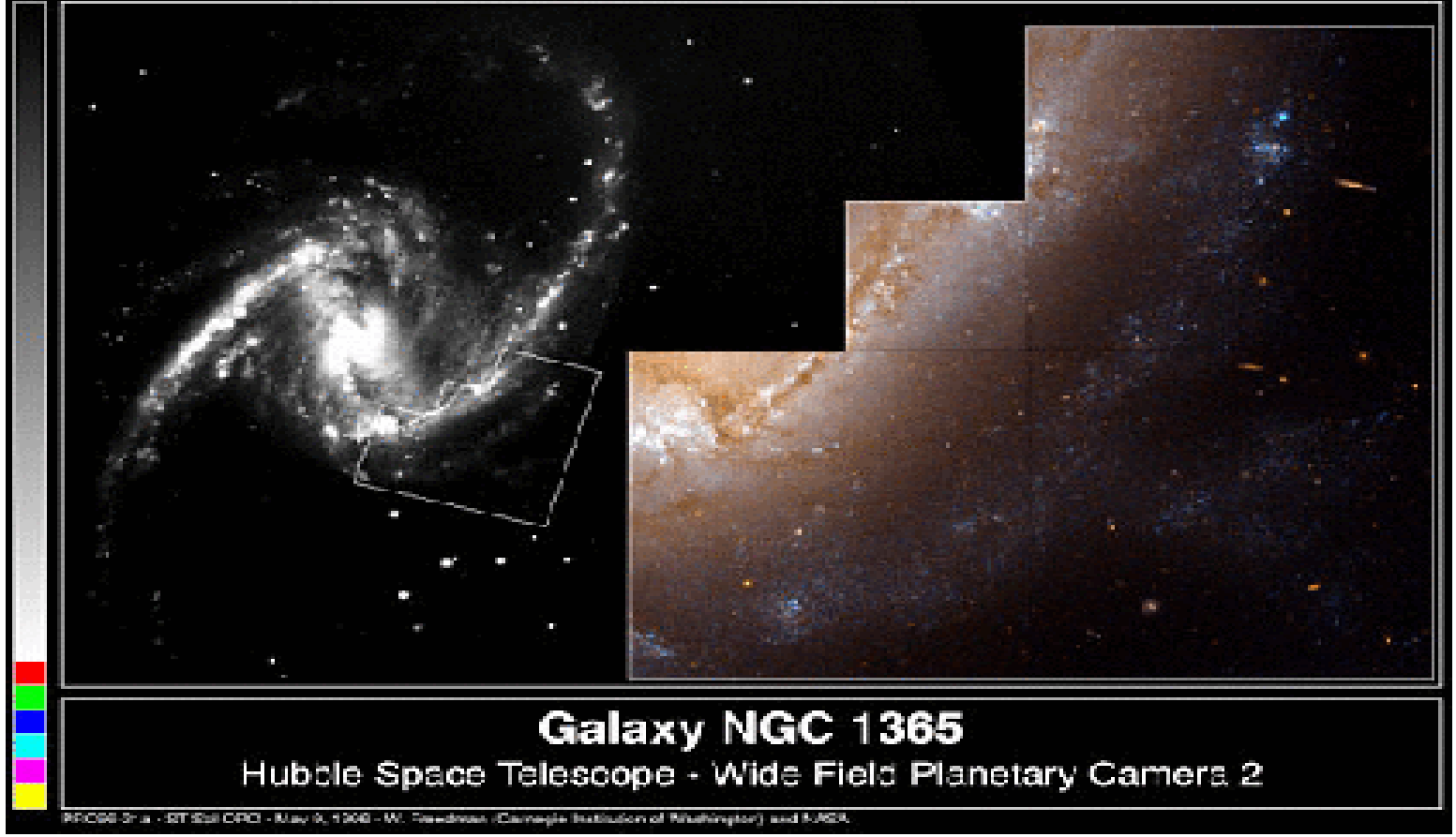

Barred Spiral Galaxy NGC 1365

IMAGES OF A GALAXY IN THE FORNAX CLUSTER OF GALAXIES

This colot image from the Hubble Space Telescope shows a tegion in NGC 1365, a batred spital galaxy located in a clustet of galaxies called Fotnax. A batred spital galaxy is chatacterized by a "bat" of stats, dust and gas actoss its center. The black and white photograph from a ground-based telescope shows the entite galaxy, which is visible from the Southetn Hemisphete. Membets of the Key Ptoject team, who have been measuting the distance to the Fotnax clustet, have estimated it to be 60 million light-yeats ftom Earth. The team attived at theit ptelimintty estimate by using Cepheids, bright, young stats that ate used as milepost matkets to calculate distances to neatby galaxies. The line of small blue dots in the colot image shows the fotmation of stats in the galaxy's spital atms, making them ideal

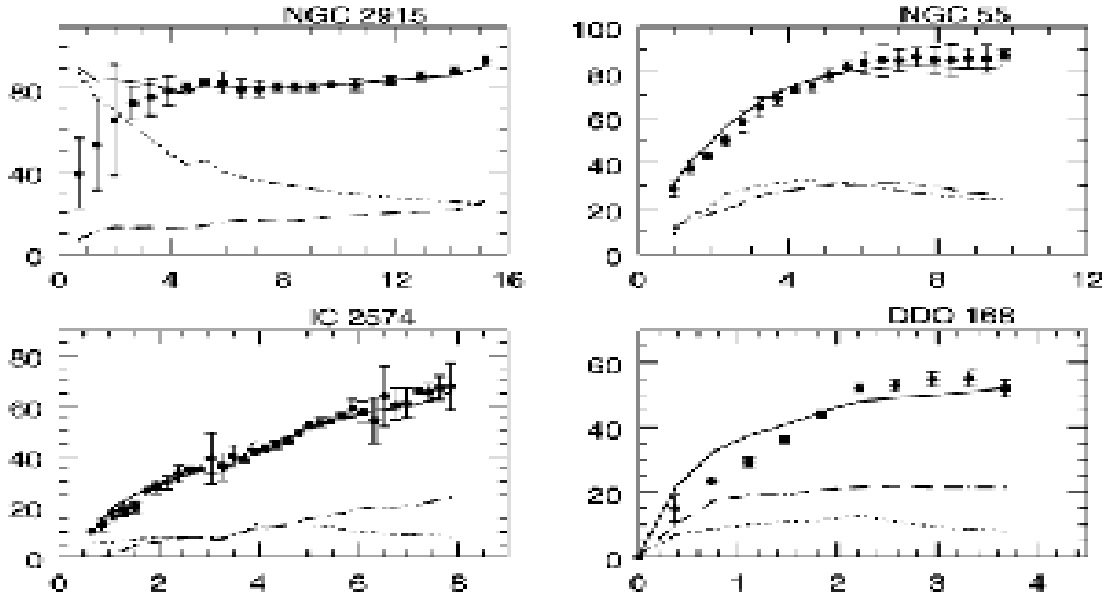

FIG. 1.—Continued

surface density is below the MOND critical surface density of a_0/G, the MOND prediction (Milgrom 1983) is that the discrepancy should be large within the optical disk and that the rotation curve should rise slowly to its asymptotic limit. This is seen to be the case, and the MOND rotation curve agrees with the observed curve in detail. It should be emphasized that the general MOND prediction of a large discrepancy in low surface density systems (Milgrom 1983) was made long before observations of systems such as this one confirmed it.

M33.—The observed rotation curve of this classic nearby Sc spiral is from an unpublished analysis by O. M. Kolkman (1995) based upon observations of Deul & van der Hulst (1987; see also Rhee 1996). The large number of independent observed points on the rotation curve, due to the large angular size this object, and the well-established Cepheid distance (Madore & Freedman 1991) make this a good case for detailed rotation-curve fitting, although there is a significant warp in the outer regions.

NGC 2915.—This is a blue compact galaxy (BCG) recently analyzed by Meurer et al. (1996). The neutral hydrogen extends well beyond the bright optical image (to 22 times the exponential scale length), and the observed rotation curve remains constant, with a suggestion of a rise at the outermost measured points. This implies a very large discrepancy between the visible and Newtonian dynamical mass (hence the authors refer to this object as the darkest disk galaxy). The MOND rotation curve is higher than the observed curve in the inner regions (where the errors are large) but agrees very well with the observed rotation curve in the outer regions. Here even the apparent rise of rotation-ratio for the disk is 69, which is an uncomfortably large value for a BCG. The distance to the galaxy is quite uncertain; Meurer et al. gave 5.3 ± 1.3 Mpc based on the method of brightest stars. At a distance of 6.6 Mpc, M/L is reduced to 3.3. It might also be that the luminosity has been underestimated if a faint luminous halo surrounds the bright, blue compact object.

DDO 168.—This is a dwarf with a small bar in the central regions. The MOND rotation curve lies noticeably above the observed rotation curve in the inner regions. This should not be given too much significance, because of the possible effects of the bar or of beam smearing.

Table 3 lists the fitted disk and bulge masses for all galaxies in the present sample, as well as those in the sample of BBS—a total of 33 galaxies for which MOND rotation curves have been calculated. Also shown are the implied mass-to-blue light ratios, for the disk and bulge separately where applicable. In column (6), the global (bulge plus disk) mass-to-light ratio in the blue is given for the luminous (stellar) component, M^*/L_B; in column (7), the ratio of the total mass (stars plus gas) to luminosity in the blue band is given (M_g/L_B); in column (8), the ratio of the total mass to luminosity in the H band (M_t/L_H) is given for those galaxies for which an H-band magnitude has been measured. It should be noted that the fitted mass, M^*, includes not only the mass in luminous stars but also any other component that is distributed like the stars, such as, possibly, the molecular gas.

We see that in most cases the global mass-to-light ratios are reasonable and consistent with population synthesis

Dark Matter

- From the stellar motion near the Sun, the mass needed to provide the gravity is more than the observed mass.
- The missing mass problem
- The rotation curves
- The gravitational lens
- Dark Matter Candidates: Neutrino, Axions

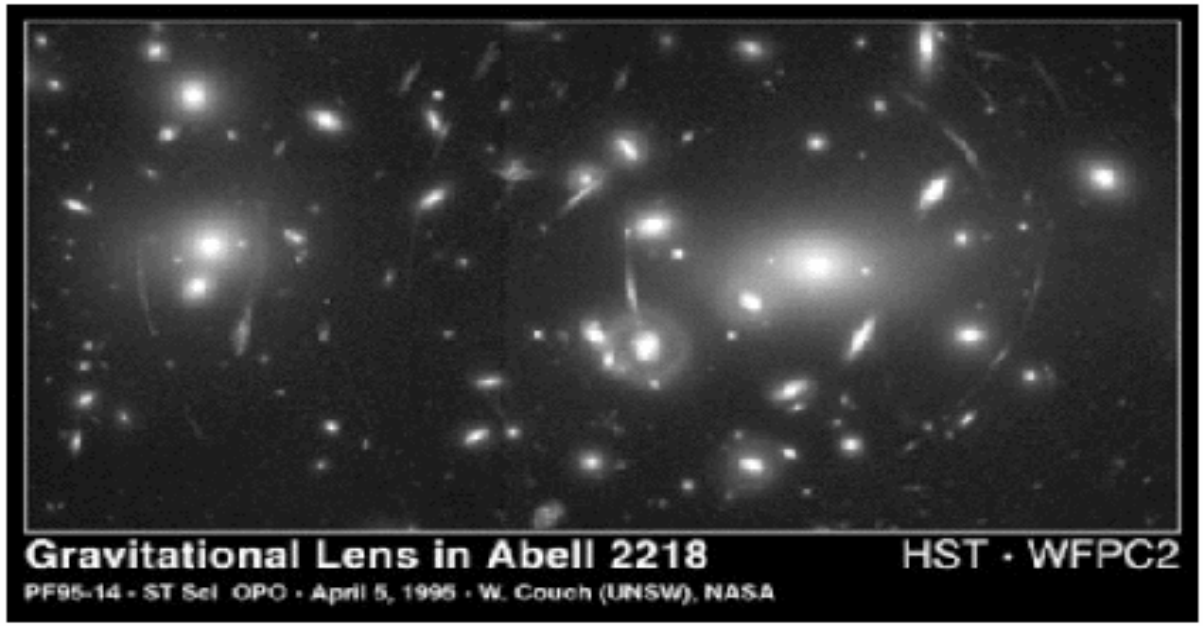

Gravitational Lensing in Galaxy Cluster Abell 2218

HUBBLE VIEWS DISTANT GALAXIES THROUGH A COSMIC LENS

This NASA Hubble Space Telescope image of the rich galaxy cluster, Abell 2218, is a spectacular example of gravitational lensing. The arc-like pattern spread across the picture like a spider web is an illusion caused by the gravitational field of the cluster.

The cluster is so massive and compact that light rays passing through it are deflected by its enormous gravitational field, much as an optical lens bends light to form an image. The process magnifies, brightens and distorts images of objects that lie far beyond the cluster. This provides a powerful "zoom lens" for viewing galaxies that are so far away they could not normally be observed with the largest available telescopes.

Hubble's high resolution reveals numerous arcs which are difficult to detect with ground-based telescopes because they appear to be so thin. The arcs are the distorted images of a very distant galaxy population extending 5-10 times farther than the lensing cluster. This population existed when the universe was just one quarter of its present age. The arcs provide a direct glimpse of how star forming regions are distributed in remote galaxies, and other clues to the early evolution of galaxies.

Hubble also reveals multiple imaging, a rarer lensing event that happens when the distortion is large enough to produce more than one image of the same galaxy. Abell 2218 has an unprecedented total of seven multiple systems.

The Warped Galaxies

- About 1/3 to half of the disc galaxies are warped
- Our Galaxy, the Milky Way, is warped
- M31 is warped
- Sancisi (1976): four of a sample of five edge-on galaxies have warped disc,
- Three of them are isolated

M 31
The Andromeda Galaxy

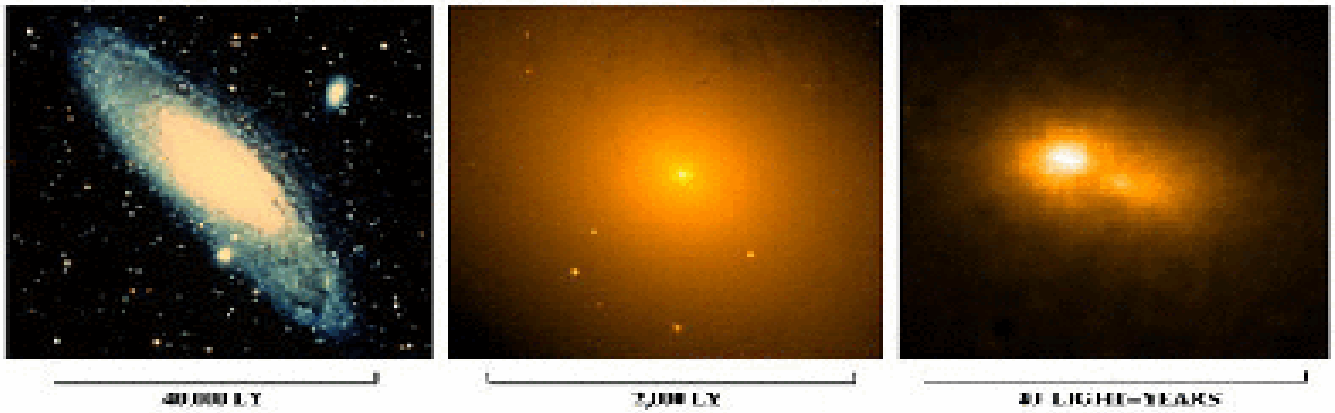

Ground View of Galaxy | Ground View of Galaxy Core | HST View of Galaxy Nucleus

Composite of M31 Images

DOUBLE NUCLEUS OF THE ANDROMEDA GALAXY M31 [three-frame]

[Right] HST VIEW OF GALACTIC NUCLEUS

A NASA's Hubble Space Telescope image of a "double nucleus" in the giant spital galaxy in Andromeda, M31.

Each of the two light-peaks contains a few million densely packed stars. The brighter object is the "classic'' nucleus as studied from the ground. Howevet, HST reveals that the true center of the galaxy is really the dimmet component.

One possible explanation is that the brightet cluster is the leftovet temnant of a galaxy

Letter to the Editor

Warped H I Disks in Galaxies

R. Sancisi

Kapteyn Astronomical Institute University of Groningen, Groningen 8002, The Netherlands

Received September 16, 1976

Summary

Hydrogen-line observations of nearby edge-on galaxies with the Westerbork Synthesis Radio Telescope have revealed a significant bending of the outer gas layers in four out of five systems. Three of these systems are fairly isolated in the sky. The most pronounced and unambiguous warp is found in NGC 5907, where the deviation of the HI layer from the optical plane is about 20 percent of the radius.

Key-words: Galaxies – Neutral Hydrogen.

Introduction

External galaxies with warped optical disks have been known for a long time. Well-known examples are NGC 3190 (cf. Arp 1966) and NGC 4762 (cf. Sandage 1961); another is NGC 5866 (cf. Sandage 1961), where the tilt of the absorption lane was already noticed by Pease (1917). However, these seemed to have been regarded as rare cases, probably resulting from gravitational interactions. About two decades ago a similar large-scale bending was discovered in the outer parts of the gas layer of our Galaxy (Burke 1957, Kerr 1957). A number of explanations were proposed to explain this warp, the most favoured being the hypothesis of a recent tidal interaction with the Large Magellanic Cloud (cf. Hunter and Toomre, 1969).

In recent years, high spatial resolution 21-cm studies of external galaxies have suggested that the neutral hydrogen layers of some other systems may be likewise warped. The two most impressive examples are probably M33 (Kerr and Westerhout 1965; Newton 1971; Wright, Warner and Baldwin 1972; Rogstad, Wright and Lockhart 1976) and M83 (Lewis 1968; Rogstad, Lockhart and Wright 1974). However, neither of these galaxies is viewed edge-on, hence their warps have largely had to be inferred from kinematic models rather than observed directly.

New evidence on warps now comes from a 21-cm line survey of five edge-on galaxies carried out with the Westerbork radio telescope. This survey reveals one striking case of bending in NGC 5907 and two instances of milder distortion in NGC 4565 and 4244; it also shows a warped and much disturbed hydrogen layer in NGC 4631 (Weliachew, Sancisi and Guélin 1976, in preparation) and an essentially flat disk in NGC 891 (Sancisi, Allen and Van Albada 1974). Here we report the main results on NGC 5907, 4565 and 4244; the observations will be discussed in more detail in a separate publication. Results of previous, incomplete and lower-sensitivity observations, showing the bending on the northern side of NGC 5907, have already been reported by Guélin, Sancisi, Weliachew and Van Woerden (1974).

NGC 5907

The evidence for the warp of NGC 5907 is illustrated in the first two figures. Figure 1 shows the distribution of brightness temperature of neutral hydrogen in two velocity channels, superposed on a photograph of NGC 5907. A larger sample of maps has been collected in Figure 2 to illustrate the bending at different velocities. In this diagram the channel maps appear in order of increasing rotational speed from the left to the right; not shown are other maps for the intermediate velocities 540 – 800 km/s, nor four extra maps for the very most extreme velocities 400, 420, 920 and 940 km/s. These observations

Fig. 1

Two channel maps of neutral hydrogen receding and approaching with almost maximum rotational speed, superposed on a photograph of NGC 5907. The photograph is from two stacked IIIa J plates taken by Van der Kruit and Allen with the 48" telescope of the Palomar Observatories. The contours show the distribution of beam-averaged brightness temperature at 3 (= 3σ, dashed), 6, 8, 12, 16, 20 K. The velocity channels at and near the systemic velocity are not shown; this accounts for the gap in the radio map towards the centre. The velocities are heliocentric. The beam-width at half-power (dotted ellipse) is 51" x 61". North is at the top, east on the left

How could warps form ?

- Lynden-Bell (1965): small difference between the angular momentum vector and the galaxy's symmetry axis
- Hunter & Toomre (1969): treated as an eigen value problem. For the real galaxies, the only discrete normal mode is the trivial mode: a tilt in the plane of the whole disc
- Toomre (1983), Dekel & Shlosman (1983): the trivial discrete normal mode can become non-trivial if there is a dark halo.

The Normal Mode

Sparke & Casertano (1988): assuming a fixed flattened dark halo, they use normal modes to fit the shape of galaxies, say, NGC 4013

Nelson & Tremaine (1995): using analytic perturbation theory to study the energy transfer between warp & dark halo. They claimed the warp shall decay.

Binney, Jiang & Dutta (1998)

- Using N-body simulations to study the effects of the live halo
- In fact, the disc-disc, disc-halo, halo-halo interactions are all considered
- The goal is to study the fate of normal mode
- We reproduce the normal mode when we fix the halo particles (thus halo potential)

We actually inherit all the above and we also include the gravitational force of the halo to calculate Ω as a modification of assumption 2.

The vertical dynamics of the disc is described by:

$$\left[\frac{\partial}{\partial t}+\Omega\frac{\partial}{\partial \phi}\right]^2 z(t,r,\phi) = -\frac{\partial \Phi_{\rm h}}{\partial z} + f, \tag{2.1}$$

where Ω is the circular frequency, $\Phi_{\rm h}$ is the halo potential and f is the vertical force per unit mass due to other parts of the disc. To understand the physical picture behind this equation, let's rewrite Hunter & Toomre's words about f here:

"One should regard the later force (f) as a mass average of the actual vertical forces experienced by different *parcels of material* at, above or below the reference point r, θ."

Note that they use *parcels of material* to refer to the objects to which the forces apply in the equation. This is the way in which cosmologists simulate large scale structure by considering galaxies with 10^{11} stars as single dots. That is, we actually consider a group of stars with gas or say, galactic material as the object in the disc plane. Binney et al. (1998) and Smart et al. (1998) just say "a star" for convenience but what they mean by a star is a bunch of stars that are located in the same volume of space and have very similar velocities because Binney et al. employ a softening parameter for their disc self-gravity calculation (See Binney & Tremaine 1987 page 91 for this concept.) and Smart et al. actually use the median values of velocities to compare with the theoretical prediction.

For the linear case, i.e. $|z(t,r,\phi)| \ll r$ for any r, the halo force can be expanded as:

$$-\frac{\partial \Phi_{\rm h}}{\partial z} = -\frac{\partial \Phi_{\rm h}}{\partial z}\Big|_{z=0} - z\frac{\partial^2 \Phi_{\rm h}}{\partial^2 z}\Big|_{z=0} + {\rm O}(z^2) \simeq F_{\rm h} - \kappa_z^2 z, \tag{2.2}$$

where

The vertical force f due to the disc self-gravity is given, to first order in $|z(t,r,\phi)|/r$, by

$$f(t,r,\phi) = \int_{r'=0}^{\infty}\int_{\phi'=0}^{2\pi} G\Sigma_d(r')r'dr'\frac{[z(t,r',\phi') - z(t,r,\phi)]d\phi'}{\Delta(r,r',\phi'-\phi)}, \tag{2.4}$$

where Σ_d is the disc surface density and

$$\Delta(r,r',\theta) \equiv (r^2 + r'^2 + a^2 - 2rr'\cos\theta)^{3/2}. \tag{2.5}$$

Here a is the softening of the force and its value is about the thickness scale of the disc.

Since we are going to solve these equations numerically and the resolution in r-direction is not infinite, we cut the disc into a number of circular belts. The disc surface density can then be written as

$$\Sigma_d(r) = \sum_i m_i \frac{\delta(r-r_i)}{2\pi r_i}, \tag{2.6}$$

where m_i is the mass of the belt of radius r_i. We then express the vertical displacement at any radius (belt) as a Fourier series, i.e.

$$z_i(t,\phi) = \sum_{m=0}^{\infty} z_{cmi}(t)\cos(m\phi) + z_{smi}(t)\sin(m\phi), \tag{2.7}$$

where the index i has replaced r as radius parameter since we have cut the disc into discrete belts. We thus use this notation hereafter for some variables and the equations of motion of the disc. However, if we would like to emphasize a particular variable is a function of r when we derive or state the equations for this variable, we still use r as radius parameter. For example, $\kappa_z^2(r)$ is actually equivalent to κ_{zi}^2.

$$+z_{\mathrm{sm}i}\left(\sum_j z_{\mathrm{sm}j} f^{(a)}_{mij} + z_{\mathrm{sm}i}\sum_j f^{(b)}_{ij}\right) + \Omega^2_{\mathrm{dm}i} z^2_{mi}\Big]. \tag{2.22}$$

Here we have defined $\Omega_{\mathrm{hm}i} \equiv m\Omega_{\mathrm{h}i}$ and $\Omega_{\mathrm{dm}i} \equiv m\Omega_{\mathrm{d}i}$ for convenience and

$$z^2_{mi} \equiv z^2_{\mathrm{cm}i} + z^2_{\mathrm{sm}i}. \tag{2.23}$$

2.2 Halo

We represent the halo by an ensemble of particles that move in the combined potential of the halo and disc. We expand the halo potential and its density in spherical harmonics as follows,

$$\begin{aligned}
\rho_{\mathrm{h}}(r,\theta,\phi) &= \sum_{l=0}\sum_{m=0}^{l} p_l^m(\cos\theta)[A_{lm}(r)\cos(m\phi) + B_{lm}(r)\sin(m\phi)], \\
\Phi_{\mathrm{h}}(r,\theta,\phi) &= \sum_{l=0}\sum_{m=0}^{l} p_l^m(\cos\theta)[C_{lm}(r)\cos(m\phi) + D_{lm}(r)\sin(m\phi)].
\end{aligned} \tag{2.24}$$

Here the p_l^m are defined in terms of the conventional Legendre functions P_l^m by

$$p_l^m \equiv \sqrt{\frac{(l-|m|)!}{(l+|m|)!}} P_l^m\,. \tag{2.25}$$

We use p_l^m as the Legendre functions in this thesis to simplify the equations except in the Section 3.4.2 where there is no advantage to use p_l^m. However, since

$$p_l^0 = P_l^0 \equiv P_l, \tag{2.26}$$

we use P_l rather than p_l^0 as our convention.

The C_{lm} are related to A_{lm} by (Bontekoe 1988)

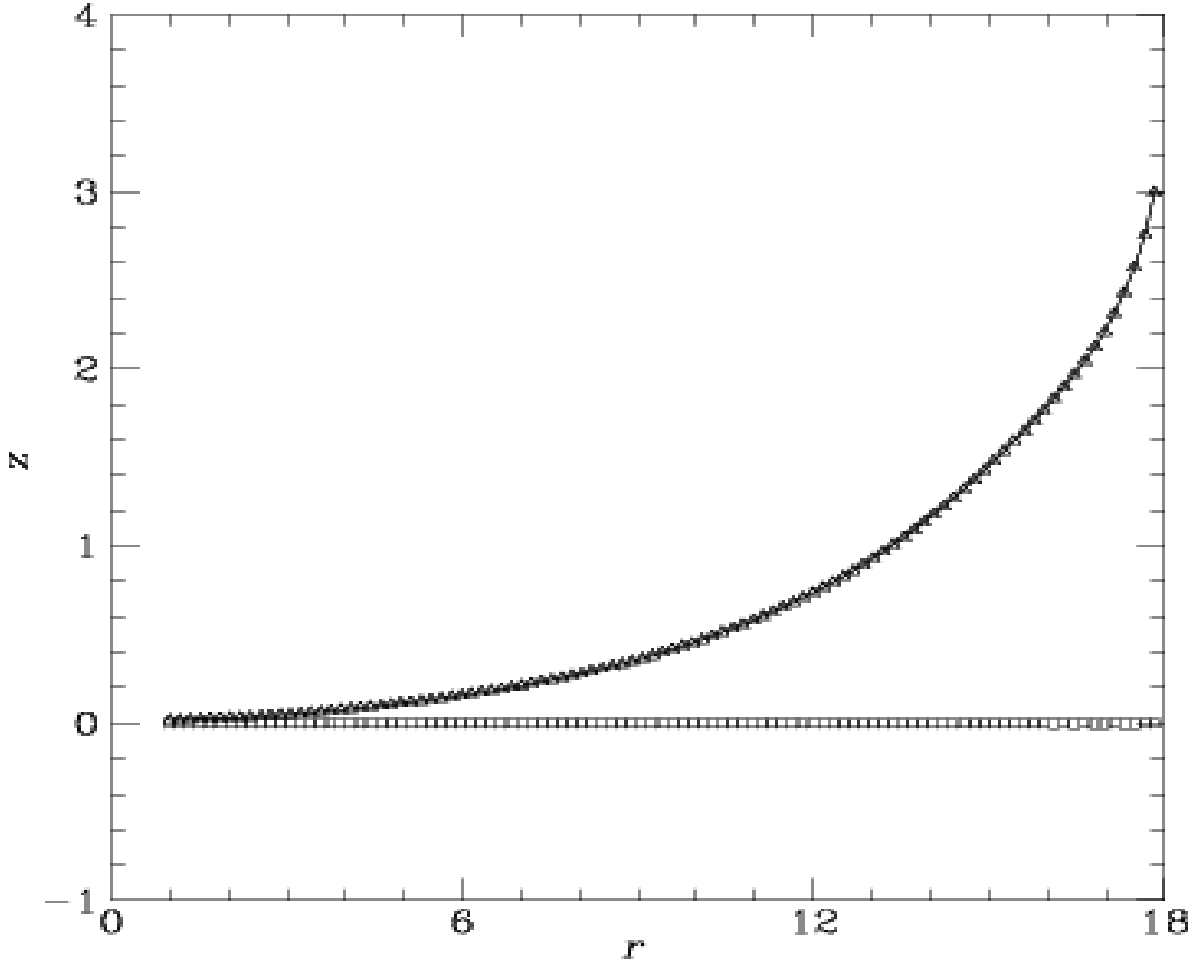

Figure 4.2: Plots of $z(t, r, \phi = \Omega_p t)$ for $t = 0$ (curve) and $t = 2000$ (triangles) when the disc is allowed to evolve from the configuration of a normal-mode for time t in a frozen halo ($2000\Omega_p = 164°$). The open squares show $z(t, r, \phi = \Omega_p t + \frac{1}{2}\pi)$ at $t = 2000$. (The corresponding values of z for $t = 0$ are identically zero.)

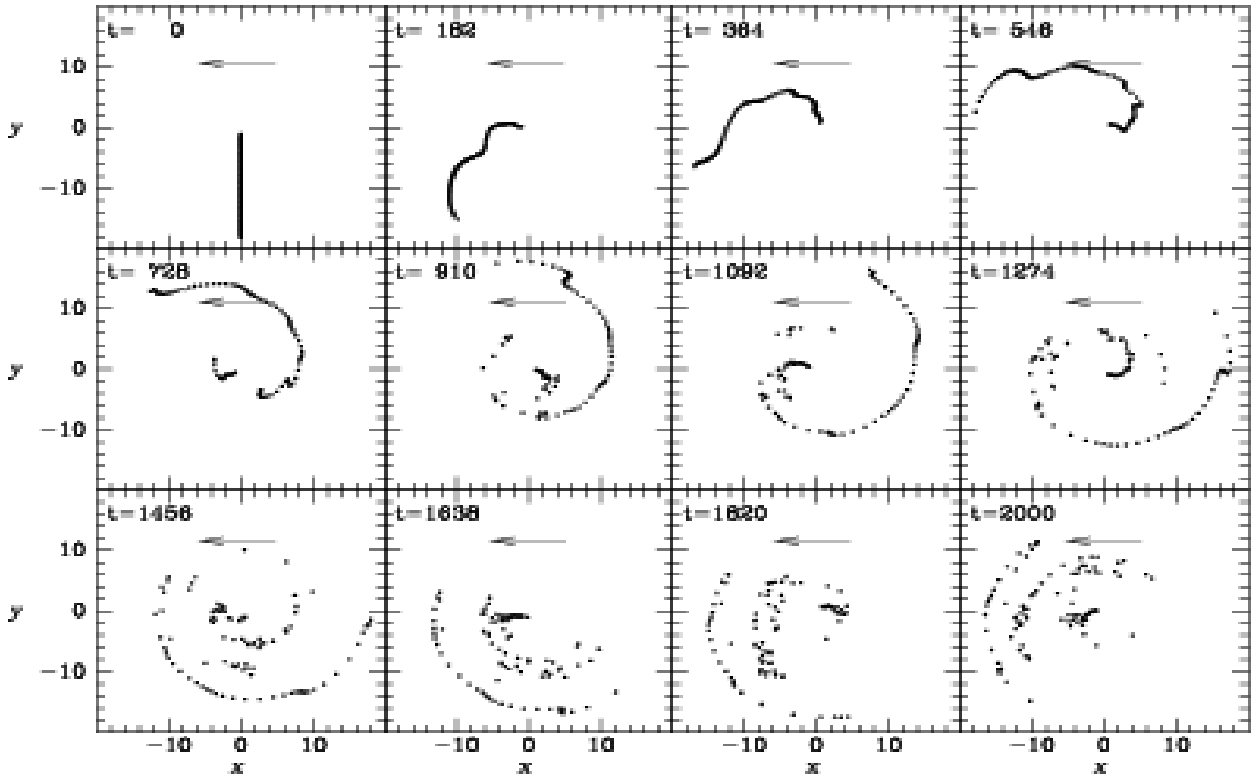

Figure 4.5: A warp in a live halo rapidly winds up even though its initial configuration would be a normal mode if the halo were static. Here we plot at several times the curve of nodes that is defined by $\phi(r) = \pi + \mathrm{atan2}[z_c(r), -z_s(r)]$ for a live disc that evolved in a live halo from a configuration that was a normal mode in the sense of Sparke & Casertano. The arrow in each panel indicates that the disc is rotating anticlockwise.

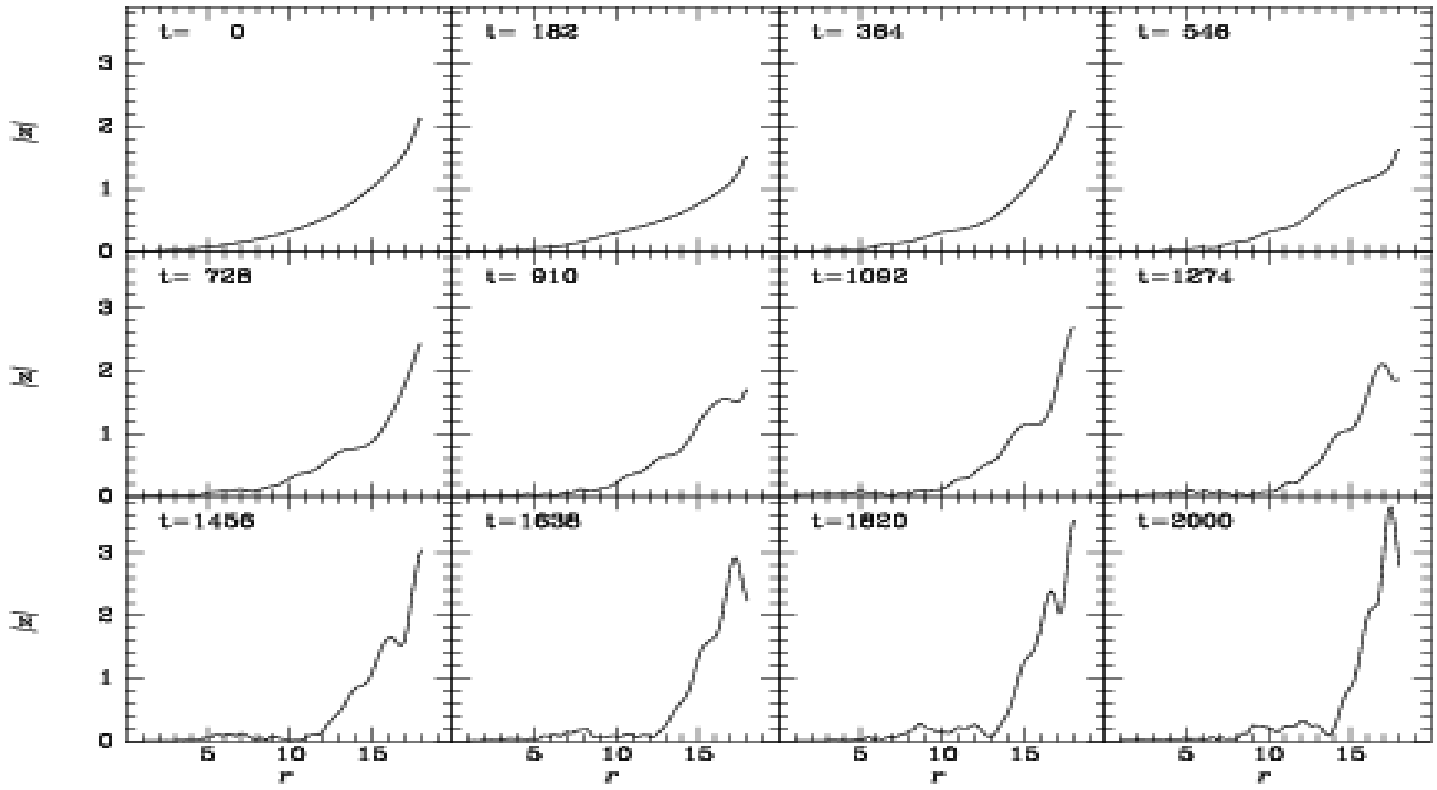

Figure 4.6: The rms vertical displacement $|z| = \sqrt{\frac{1}{2}(z_c^2 + z_s^2)}$ as a function of radius for the simulation whose curves of nodes are shown in Figure 4.5.

Jiang & Binney (1999)

- The net angular-momentum vector of a galactic dark halo must significantly shift its direction every Hubble time
- There are secondary cosmic infall to re-orientate the angular momentum
- We show that this cosmic infall could produce warps if massive & gentle

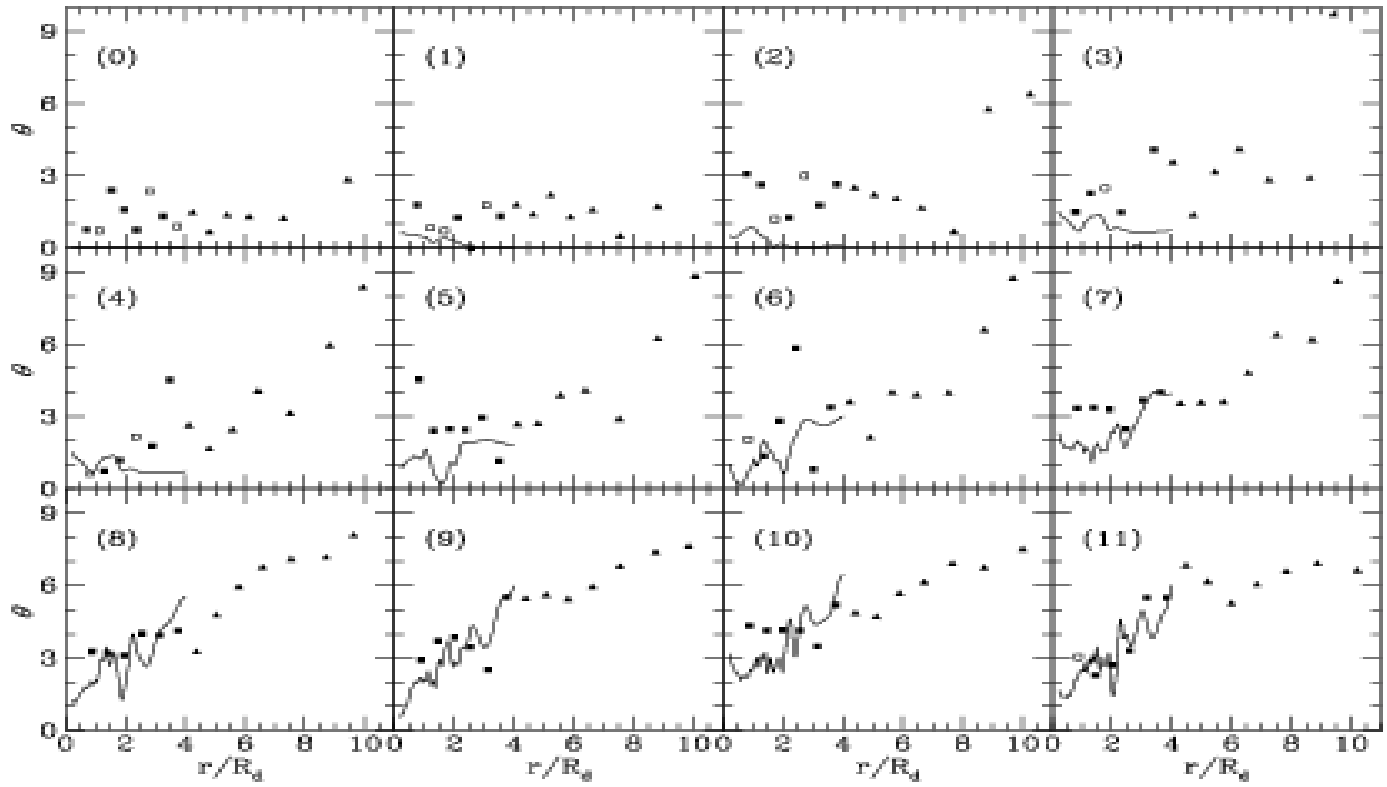

Figure 5.1: In each panel the curve shows, as a function of radius, the inclination $\theta_{\rm d}$ of the disk to its original symmetry axis while the points show the inclination $\theta_{\rm h}$ of the halo to the same axis. Filled symbols indicate that the halo is inclined in the same sense as the disk, and open symbols indicate the opposite sense of inclination. Beyond the edge of the disk, the halo's inclination is marked by triangles. Between successive panels a time has elapsed which is equal to ~ 2.3 times the time, $t_{\rm rel}$, required to travel the halo's half-mass radius at the rms speed of a halo particle. In this simulation the halo has no net rotation.

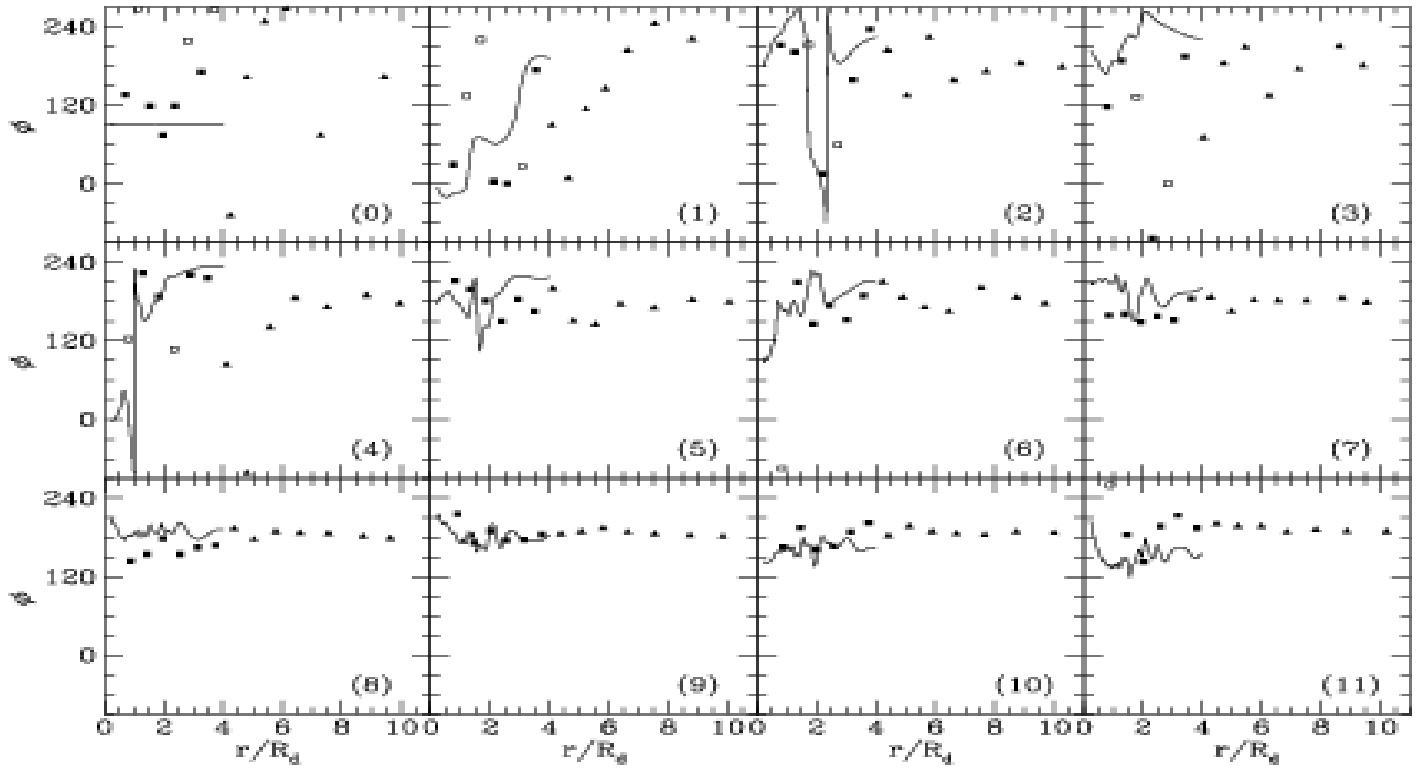

Figure 5.2: In each panel the curve shows, as a function of radius, the azimuth angle ϕ_d of the disc while the points show the azimuth angle ϕ_h of the halo. Filled symbols indicate that the halo is inclined in the same sense as the disk, and open symbols indicate the opposite sense of inclination. Beyond the edge of the disk, the halo's inclination is marked by triangles. Between successive panels a time has elapsed which is equal to ~ 2.3 times the time, t_{rel}, required to travel the halo's half-mass radius at the rms speed of a halo particle. In this simulation the halo has no net rotation.

Jiang & Binney (2000)

- The Sgr Dwarf Galaxy, only 20 kpc from the Galactic Center (Ibata et al. 1994)
- The current mass is about 10^9 Solar Mass
- The current orbital period is 0.76 Gyr
- The stars of Sgr Dwarf Galaxy are older than 10 Gyrs old
- It shall have dissolved
- Zhao (1998): encountered with LMC ?
- Ibata & Lewis (1998) disagreed
- We consider Dynamical Friction & Mass Lost

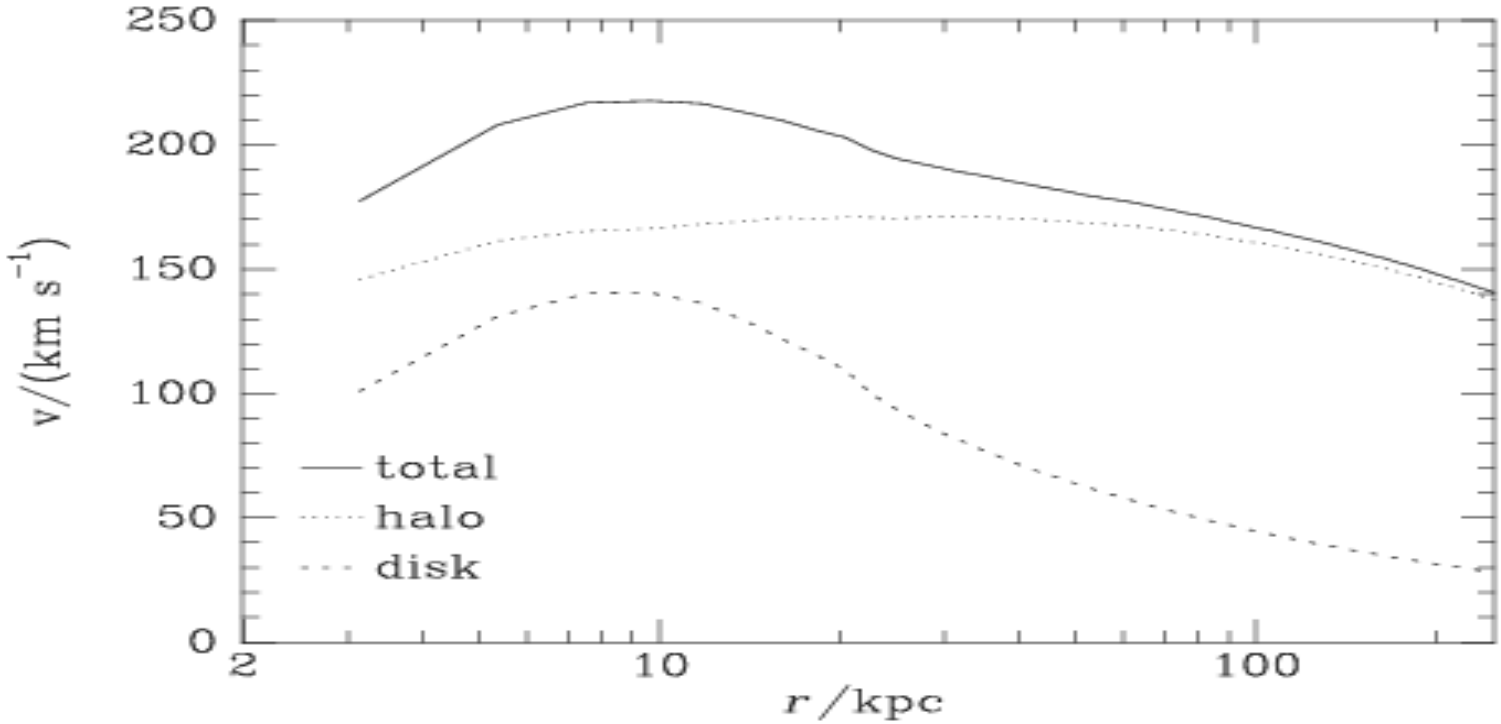

Figure 6.1: The circular-speed curve of the Milky Way and its decomposition into contributions from the disc and halo.

with harmonics up to $l = 8$ included. This done, the potential at any point can be obtained from equation (2-122) of Binney & Tremaine (1987). Our code differs from that of Bontekoe in the following ways.

1. Both the angular and the radial grids are adaptive. The radial grid points move so that roughly equal numbers of particles lie in each interval of the radial grid. Within each radial bin, a grid in colatitude θ is established that has roughly equal numbers of particles in each bin, and within each of these bins a grid in azimuth ϕ is established that has equal numbers of particles in each bin.

$$M_{\rm D}(t, r_{\rm t}) = 4\pi\, D(t) \int_0^{r_{\rm t}} {\rm d}r\, r^2 \rho_{\rm D}(r), \tag{6.8}$$

where $\rho_{\rm D}(r)$ is the Dwarf's initial density profile [equation (6.3)] and

$$D(t) = \frac{1}{\tanh(\beta)} \tanh\left(\beta[r_{\rm t}(t)/r_{\rm t}(0)]\right) \tag{6.9}$$

is the *Dilution Function* that takes into account the tendency of tidal stripping to decrease the density even inside the tidal radius because some tidally stripped stars initially spent time at small radii. β is a parameter that controls the speed with

Table 6.2 Orbits

Orbit	$M_{\rm D\infty}$ $/10^{10}M_\odot$	$M_{\rm D}(0)$ $/10^{10}M_\odot$	$r_{\rm Dt}$ /kpc	$r_{\rm D\infty}$ /kpc	$R_{\rm D}$ /kpc	$t_{\rm simk}$ /Gyr	$M_{\rm D}(t_{\rm simk})$ $/10^9 M_\odot$	$\sigma_{\rm D}(t_{\rm simk})$ /kms^{-1}
A	10	10	20	70	250	11.10	2.015	25.4
b	10	9.842	25	80	250	13.38	1.094	21.0
c	10	9.936	20	70	225	8.91	2.883	27.8
d	10	9.661	25	80	225	10.88	1.740	23.7
e	10	9.426	25	80	200	8.63	1.925	24.9
F	10	8.837	30	100	200	10.60	1.122	21.3
g	9	8.427	25	80	200	9.91	1.775	23.9
h	7	6.422	25	80	200	14.14	1.022	20.3
i	7	6.725	20	70	200	10.77	1.799	24.0
j	7	6.306	20	70	150	5.93	3.086	28.7
K	5	4.377	20	70	150	9.93	1.765	23.7
l	5	3.728	20	70	100	4.54	3.286	29.7
m	3	2.046	20	70	100	10.10	1.686	23.2
n	3	1.489	20	70	60	3.52	3.043	28.5
o	1.4	0.5515	20	70	60	10.49	0.9491	19.4

which the Dwarf is torn apart. If β is big, the stripping of material has little impact on the inner Dwarf until mass loss from the outside is far advanced. equation (6.8) gives an estimate of the mass of the Dwarf for any assumed value of r_t. The value of r_t is determined at each time-step by finding the radius r_t' that satisfies the usual tidal condition

$$\frac{M_D(r_t')}{r_t'^3} = \frac{M_G(r - r_t')}{(r - r_t')^3} \tag{6.10}$$

and then setting $r_t = min(r_t, r_t')$. Hence, r_t is not permitted to increase as the Dwarf moves from peri- to apo-centre. Were it allowed to increase, equation (6.8) would give rise to an unphysical increase in M_D because it neglects the sharp fall in the density that will in reality be encountered outside the smallest value that r_t has taken along the orbit: mass lost is lost for ever.

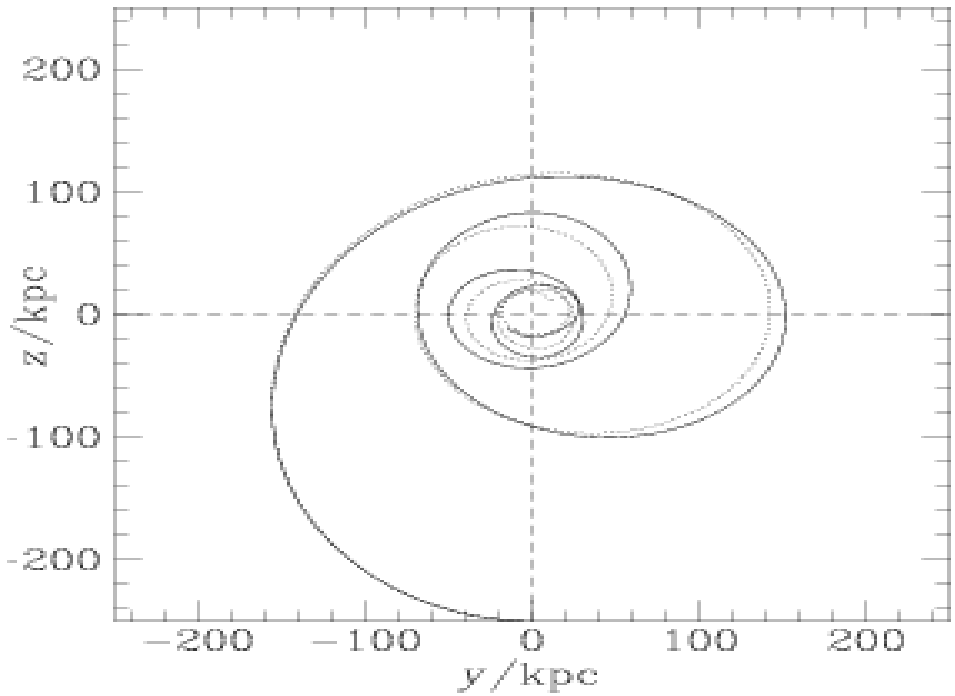

Figure 6.3: Orbit A. The full curve is obtained by full N-body simulation and the dashed curve is obtained by the semi-analytic model

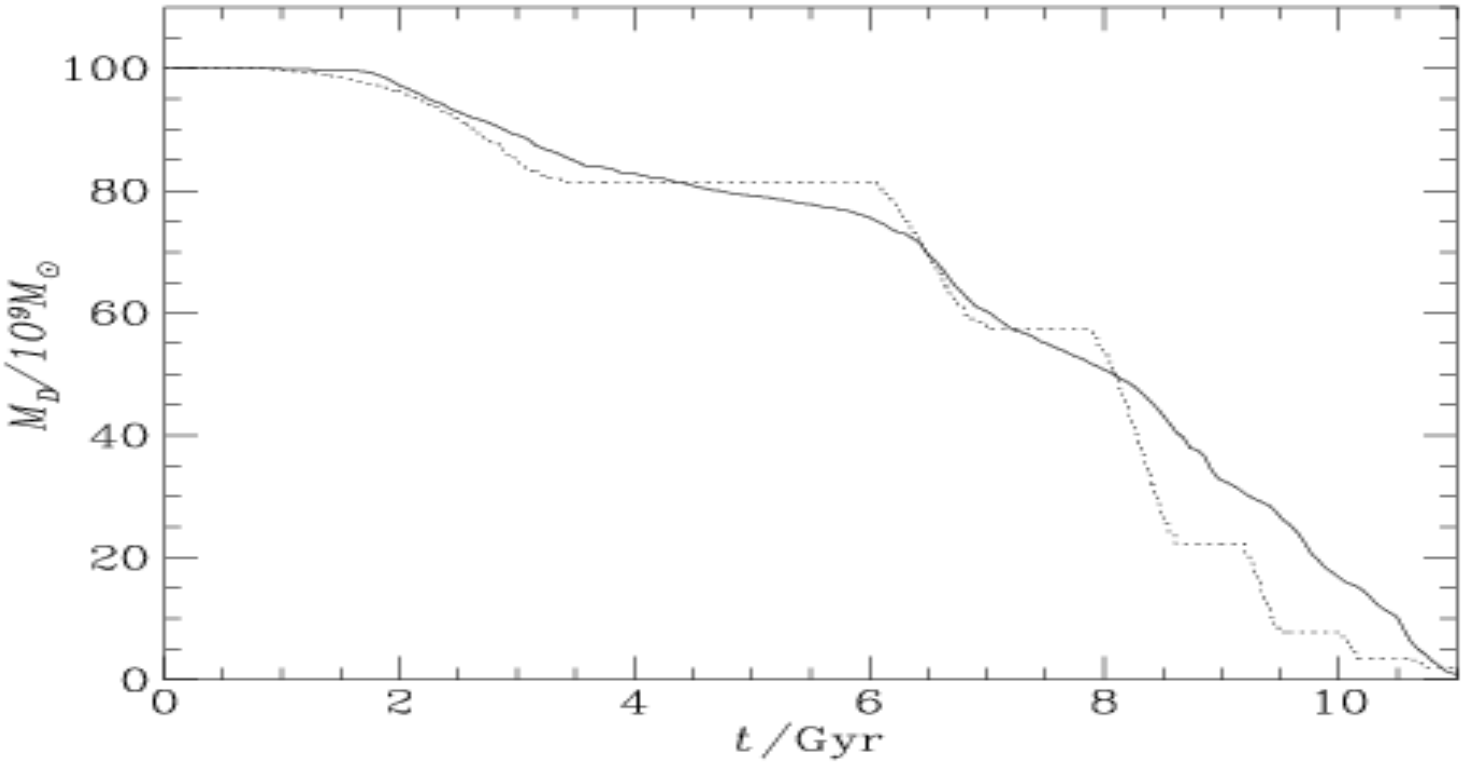

Figure 6.6: $M_{\rm D}$ as a function of t for orbit A from the N-body simulation (full curve) and from the semi-analytic model (dashed curve).

an isotropic spherical system [Binney & Tremaine equation (4-54)] with the density profile set equal to $D(t)\rho_{\rm D}(r)$. The central velocity dispersion at later time can be obtained by relating to the initial central velocity dispersion as

$$\sigma_{\rm D}(t) = \sqrt{D(t)}\sigma_{\rm D}(0). \qquad (6.11)$$

This prescription must over-estimate $\sigma_{\rm D}$ at late times because it supposes matter at $r > r_{\rm t}$ to be still bound to the system. In view of this problem, the agreement between the full and dashed curves in Figures 6.9–6.11 is satisfactory.

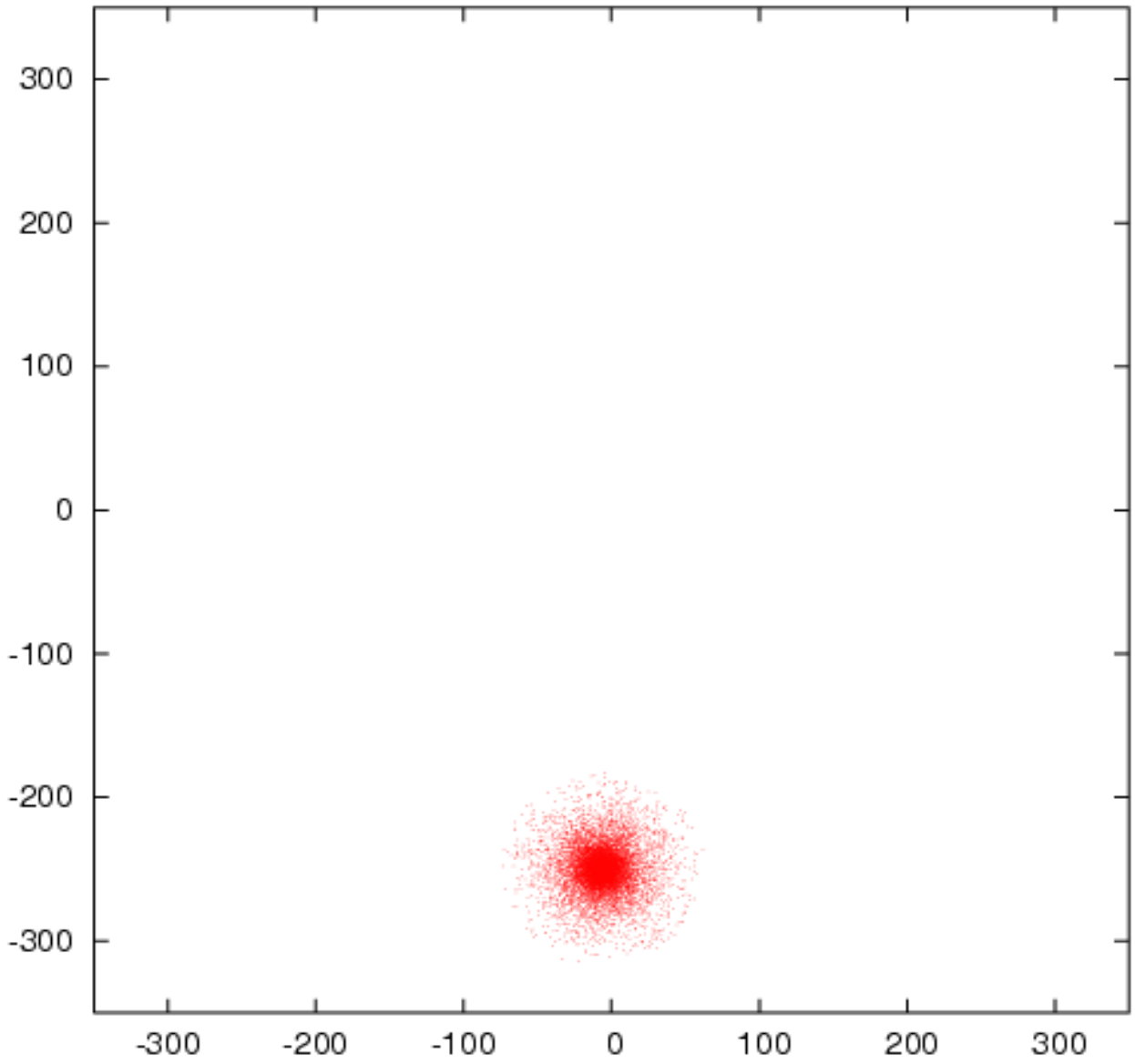
300
200
100
0
-100
-200
-300
-300
-200
-100
0
100
200
300

orbit (c),(e),(j),(l),(n) ($t_{\rm sink} < 9$). The values of $\sigma_{\rm D}(t_{\rm sink})$ for all the rest orbits are about or under 25 km/s, which is the maximum value we allow for possible orbits. The true $\sigma_{\rm D}(t_{\rm sink})$ for them would be even smaller because as we mentioned in last Section that we must over-estimate $\sigma_{\rm D}$ at late time when we integrate the Jeans equation. Moreover, Jiang & Binney (1999b) point out that the theoretical value of velocity dispersion is bigger than the measured dispersion of the Dwarf's stars because of (a) the dynamical difference between dark and luminous matter, and (b) velocity anisotropy.

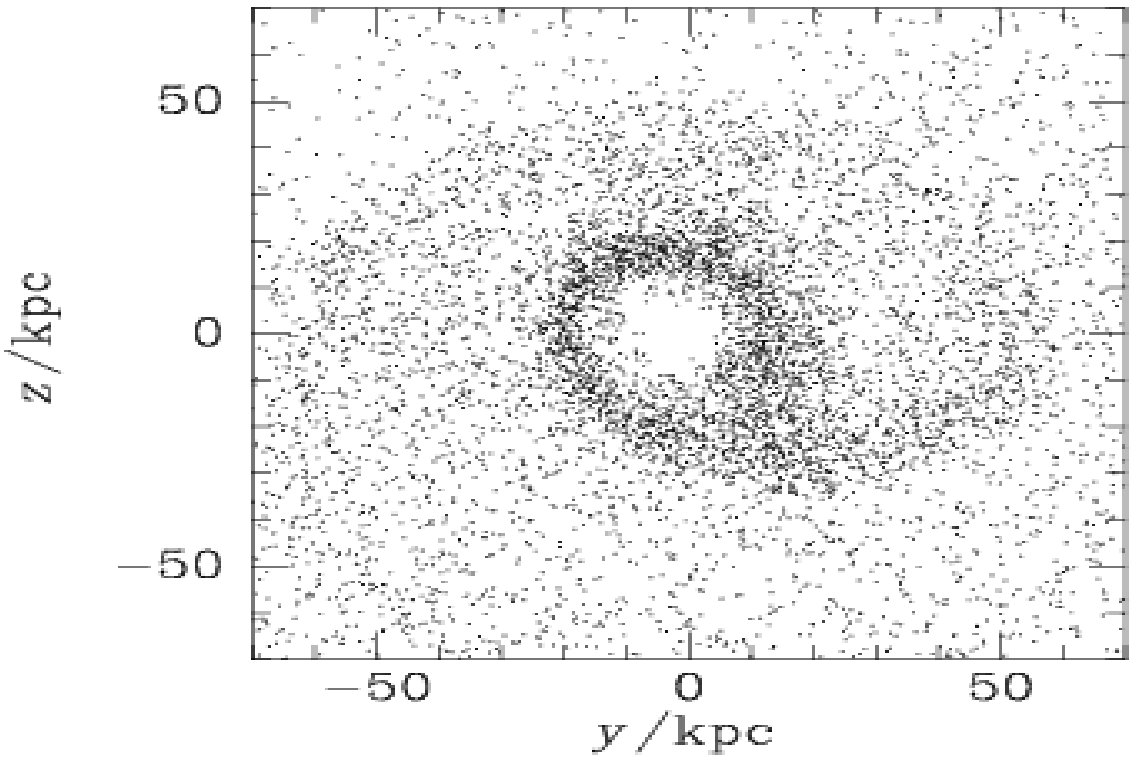

Figure 6.12: The distribution of Dwarf particles projected onto the plane perpendicular to the Dwarf's orbit for the result of Orbit A.

Modified Newtonian Dynamics (MOND)

- F = μ (x) m a, x=a/a_o, a_o= c H_o
- Newtonian Dynamics $\sim$ General Relativity
- MOND $\sim$ TeVeS ?
- Without Dark Matter, MOND has the ability to fit the Rotation Curves
- A lot more needs to be done to check whether MOND is compatible with observations of CMB, large-scale structure

Brada & Milgrom (2000)

- Using MOND & there is no dark halo
- An exponential disk & a constant external field
- The external field represents the purturber: satellite galaxy etc.
- Calculating some orbits of test particles
- They claim the warp can be produced

The Conclusions

- Our results on warps are consistent with that there are more warps for high red-shift galaxies
- The effect of a live halo is important for study of galactic dynamics
- We propose a natural possible orbit for the Sgr Dwarf Galaxy
- MOND is interesting, still attractive, but need a lot of observational tests, say, warped shapes, galactic structures, dynamics